Advance Access publication 2025 October 15



Downloaded from https://academic.oup.com/mnras/article/544/1/343/8286916 by guest on 05 November 2025

Short-lived radioisotopic enrichment from AGB interlopers in low-mass star-forming regions

Joseph W. Eatson ¹⁰1,2★ and Richard J. Parker ¹⁰1†

¹Astrophysics Research Cluster, School of Mathematical and Physical Sciences, The University of Sheffield, Hounsfield Road, Sheffield S3 7RH, UK

Accepted 2025 October 10. Received 2025 October 9; in original form 2025 August 15

ABSTRACT

The decay of short-lived radioisotopes (SLRs) can be a significant source of heating early in protoplanetary systems, though how a protoplanetary disc becomes enriched with these SLRs far above the galactic background level remains an open question. Observational evidence suggests that this enrichment occurs during the period from when the disc forms to when it progresses into a protoplanetary system, and is homogenous throughout the resultant planetary system. Whilst SLRs such as ²⁶Al and ⁶⁰Fe can be injected into discs through interaction with Wolf-Rayet winds and supernovae, these outflows can disrupt discs, and in the case of low-mass star-forming regions high-mass stars may not form at all. Recent research has determined the existence of AGB 'interlopers', asymptotic giant branch stars that pass close to or through star-forming regions that could be an alternative source of SLR enrichment to Wolf-Rayet (WR) winds and supernovae. In this paper, we study the effect of AGB interlopers on star-forming regions from a dynamical perspective, determining the enrichment amount of ²⁶Al and ⁶⁰Fe in discs within small clusters via numerous N-body simulations via a parameter space exploration. We find that enrichment is widespread from AGB stars, with efficient enrichment dependent on the time at which the interloper intersects the star-forming region. Velocity is a factor, though interlopers travelling at 30 km s⁻¹ are capable of enriching many discs in a star-forming region assuming they encounter a disc when the interloper is more evolved.

Key words: exoplanets – planets and satellites: composition – planets and satellites: formation – planets and satellites: interiors – planets and satellites: terrestrial planets.

1 INTRODUCTION

Short-lived radioisotopes (SLRs) such as ²⁶Al and ⁶⁰Fe are isotopes with half-lives on the order of 1 Myr. These isotopes have had a marked impact on the evolution of our Solar system, with their stable decay products being found throughout the Solar system within chondritic meteorites (K. Thrane, M. Bizzarro & J. A. Baker 2006; H. Tang & N. Dauphas 2012; R. K. Mishra, K. K. Marhas & Sameer 2016; A. M. Davis 2022). The decay heating from these isotopes provided the bulk of heating in the early Solar system, speeding up the process of elemental stratification in planetesimals and causing the outgassing of volatiles such as H₂O (M. M. Hirschmann et al. 2021). Outside the Solar system, the presence of these isotopes could cause desiccation of planetesimals, leading to a larger number of water-poor and rocky worlds entirely covered in an ocean. It has been found that in the case of planetesimals with similar bulk compositions to the Solar system that significant desiccation from ²⁶Al heating begins to occur at $\sim 0.1 \times$ Solar $^{26} Al$ enrichment (T. Lichtenberg et al. 2019; W. Eatson et al. 2024b). Future exoplanet-oriented space telescopes such as the PLATO (PLAnetary Transits and Oscillations

of stars) mission could potentially determine population statistics for desiccated worlds and ocean worlds via radius and bulk density estimations (T. Lichtenberg et al. 2019).

Due to the short-lived nature of these isotopes and homogeneous distribution throughout the Solar system, it is likely that SLRs are injected into a star systems protoplanetary disc within a few Myr of formation from a source within the star-forming region (R. Trappitsch & F. J. Ciesla 2015; S. J. Desch et al. 2022). The primary mechanisms of SLR injection that have been studied are through early-type stars, particularly ones with a Wolf-Rayet phase. Evolved early-type stars can dredge-up substantial quantities of ²⁶Al from their cores and eject them into the surrounding medium through their dense, fast winds (M. Arnould, G. Paulus & G. Meynet 1997). Once the massive star undergoes supernova, substantial quantities of both ²⁶Al and ⁶⁰Fe are ejected into the surrounding medium, providing a significant enrichment mechanism for 60 Fe (M. Limongi & A. Chieffi 2006, 2018). Previous simulations have shown that supernovae (SNe) and Wolf-Rayet (WR) winds can result in the observed Solar system levels of enrichment in a significant fraction of discs, however, the Solar system is on the upper end of both ²⁶Al and ⁶⁰Fe enrichment (R. J. Parker et al. 2023; J. W. Eatson, R. J. Parker & T. Lichtenberg 2024a).

Wind and SNe injection are relatively straightforward explanations of SLR enrichment; however, there are some caveats. Most impor-

²Lunar & Planetary Laboratory, University of Arizona, Tucson, AZ 85721, USA

^{*} E-mail: jweatson@arizona.edu

[†] Royal Society Dorothy Hodgkin Fellow.

344

tantly, wind-based injection is heavily biased in favour of producing lighter elements such as ²⁶Al, leading to ⁶⁰Fe enrichment being dominated by SNe-based injection (M. Limongi & A. Chieffi 2006). As noted in our previous papers and stellar evolution simulations of SNe SLR vields (M. Limongi & A. Chieffi 2018; R. J. Parker et al. 2023; J. W. Eatson et al. 2024a), stars with a mass of $M_{\star} < 25 \, M_{\odot}$ undergo supernovae, with more massive stars directly collapsing into black holes. Assuming that stars form in a star-forming region at roughly the same time, this puts the first supernovae occurring in the region at ≈ 8 Myr after initial collapse, at which point most discs have progressed to protoplanetary systems, and would not efficiently sweep up SLRs. Additionally, interactions with winds and photoionizing radiation from nearby massive stars would cause significant disruption of gas within a disc, which would inhibit the formation of gas giants (F. Concha-Ramírez et al. 2019; R. B. Nicholson et al. 2019; R. J. Parker, R. B. Nicholson & H. L. Alcock 2021). *N*-body simulations incorporating a photodissociation model show that even limited close passes can significantly disrupt a disc's typical formation (M. Patel et al. 2023). However, cloud shielding could protect the nascent protoplanetary disc from external photoevaporation during the crucial early-formation stage (L. Qiao, G. A. L. Coleman & T. J. Haworth 2023; G. A. L. Coleman, T. J. Haworth & L. Qiao 2025). Stellar feedback and shocks from the SNe would also contribute to significant disc disruption as well. Finally, due to the rarity of high-mass stars, smaller, lower mass star-forming regions may lack stars of sufficient mass entirely (R. B. Nicholson & R. J. Parker 2017).

Cosmic ray spallation from the planetary systems star could also replenish SLRs, though this replenishment only covers ²⁶Al and is not sufficient and would be inhomogeneous within the disc, which is not observed in our Solar system (R. Trappitsch & F. J. Ciesla 2015).

SLRs can also be inherited from the disc's parent molecular cloud, but would likely result in insufficient SLR quantities due to their rapid decay time-scale relative to the collapse of the molecular cloud. Galactic chemical evolution, however, can also be used to explain the presence of low-concentration SLRs such as ⁵³Mn, ¹⁰⁷Pd, and ¹⁸²Hf. Sequential star formation-based enrichment (M. Gounelle & A. Meibom 2008; M. Gounelle & G. Meynet 2012; M. Gounelle 2015) could result in higher levels of enrichment over the Galactic background. However, recent stellar evolution models (M. Limongi & A. Chieffi 2018; T. Ertl et al. 2020) suggest that the time-scales involved would be too long and the requirement for subsequent generations to form one or more Wolf–Rayet stars would mean that such enrichment would be improbable, even for SLRs with a longer half-life such as ⁶⁰Fe (R. J. Parker & J. E. Dale 2016).

Instead, an alternative means of production of SLRs must be considered: interloping asymptotic giant branch stars. In an AGB star ²⁶Al is readily produced through cool bottom processes (K. M. Nollett, M. Busso & G. J. Wasserburg 2003), and ⁶⁰Fe is transferred to the star's envelope through dredge-up. These fusion products can be ejected from the star through the stellar wind into the surrounding medium, causing SLR enrichment (M. Lugaro & A. I. Karakas 2008; J. M. Trigo-Rodríguez et al. 2009). ²⁶ Al yields from an AGB star are equivalent to a WR star, while having a markedly higher 60Fe yield (A. I. Karakas 2014; A. I. Karakas & M. Lugaro 2016; M. Lugaro, U. Ott & A. Kereszturi 2018). Furthermore, these less disruptive winds and lower photoionizing flux from the AGB star will also impact disc evolution much less than WR stars and supernovae. The possibility of pollution from an AGB star as an enrichment mechanism for the Solar system has been discussed previously in the literature (M. Busso, R. Gallino & G. J. Wasserburg 1999). Although it avoids the issues with theories for SLR enrichment involving massive stars,

there is still the caveat that the probability of such an encounter would be low, especially for an intermediate-mass AGB (J. H. Kastner & P. C. Myers 1994).

Despite this, we are re-considering this mechanism as recent strides in astrometry with *Gaia* have been able to distinguish interloping stars in star-forming regions from bona fide members (C. Schoettler & R. J. Parker 2021). In particular, R. J. Parker & C. Schoettler (2023) report the discovery of an AGB interloper that passed through the young star-forming region NGC 2264 as observed by *Gaia*, and demonstrated that this interaction could enrich a protoplanetary disc to SLR levels observed in the early Solar system. Interloper candidates have been identified in other star-forming regions (C. Schoettler, private communication), and these serendipitous discoveries could mean that interlopers are more common than once thought. Despite this, a calculation for the overall probability of an AGB interloper event has yet to be performed.

Other SLRs, such as 53Mn, 107Pd, and 182Hf were also present in the early Solar system, though in much lower quantities relative to the production of ²⁶Al or ⁶⁰Fe. For the Solar system, these other SLRs can be explained by galactic chemical evolution (T. C. L. Trueman et al. 2022), and AGB interloper enrichment is not capable of self-consistently explaining all SLR enrichment. SLR enrichment of planetary systems is likely to be common (T. Lichtenberg, R. J. Parker & M. R. Meyer 2016; A. Curry et al. 2022), but the destructive effects of photoionizing radiation from massive stars may preclude gas giant formation (M. Patel et al. 2023), and therefore we require an alternative enrichment scenario for the Solar system. Another important consideration for the probability of an interloping event occurring is the relatively short length of the AGB phase relative to the lifespan of a low-mass main-sequence star; typically this phase is of the order of a few Myr, meaning an AGB candidate could pass entirely through a star-forming region without entering the phase, leading to no enrichment. Further considerations would have to be made in regard to the intercept velocity of the interloper, typical 'runaway' (>30 km s⁻¹) speeds may significantly curtail enrichment, while 'walkaway' speeds (5–30 km s⁻¹) may be more conducive to enrichment.

In this paper, we present results from a series of simulations in order to determine the range of viable intercept velocities and AGB phase time sensitivity for significant SLR enrichment due to interloping stars, with a focus on intercept velocities at or below the galactic velocity dispersion - so-called 'walkaway' stars. We expand on previous literature by examining the dynamics between the interloper and star-forming region. We also expand on the model detailed in our previous paper on SLR enrichment (J. W. Eatson et al. 2024a) by accounting for SLRs lingering in the simulation, rather than having an 'enrichment zone' around the SLR sources. While there are a variety of studies that focus on the feasibility of AGB stellar nucleosynthesis for SLR enrichment (M. Busso et al. 1999; G. J. Wasserburg, A. I. Karakas & M. Lugaro 2017), and there are studies that focus on the probability of interactions between a star-forming region and an interloping AGB star (J. H. Kastner & P. C. Myers 1994); we instead focus on the feasibility from a dynamical perspective within the star-forming region itself. As there are observed examples of an interloping AGB star (R. J. Parker & C. Schoettler 2023) it is of interest to determine the likelihood that protoplanetary discs within a star-forming region would undergo significant enrichment. It is also of interest to consider how this likelihood changes based on interloper velocity and intercept distance, as well as the size and density of the star-forming region. The paper is organized as follows. In Section 2, we discuss the methodology of this paper, in particular, how we expand on the

model used in J. W. Eatson et al. (2024a) and covering how interloper enrichment is performed in our *N*-body simulations, and how we manage interlopers with a high intercept velocity with the star-forming region. Our results for our simulation sets are detailed in Section 3, and we provide a brief discussion in Section 4. We conclude in Section 5.

2 METHODOLOGY

The simulation code is written in PYTHON, and uses the AMUSE framework for its stellar evolution and *N*-body routines (F. I. Pelupessy et al. 2013; S. F. Portegies Zwart et al. 2013; S. P. Zwart & S. McMillan 2018). The problem is split into a series of sub-steps in order to synchronize the various codes. For *N*-body simulation the BHTREE code (J. Barnes & P. Hut 1986) was used, for stellar evolution SEBA (S. F. Portegies Zwart & F. Verbunt 1996; S. Toonen, G. Nelemans & S. Portegies Zwart 2012) was utilized.

2.1 Star-forming regions

Observations (P. André et al. 2014; A. Hacar, M. Tafalla & J. Alves 2017) and simulations (S. Schmeja & R. S. Klessen 2006; M. R. Bate 2012; P. Girichidis et al. 2012) of the earliest stages of star formation suggest that stars form in filaments, which results in a spatially sub-structured distribution of the stars that form (M. Gomez et al. 1993; A. Cartwright & A. P. Whitworth 2004; N. Sánchez & E. J. Alfaro 2009). We impose sub-structure in both the spatial and velocity distributions of the stars in our simulations by using the S. P. Goodwin & A. P. Whitworth (2004) box fractal method.

We refer the interested reader to S. P. Goodwin & A. P. Whitworth (2004) and E. C. Daffern-Powell & R. J. Parker (2020) for full details of the method. We adopt a fractal dimension of D=2.0, which results in a moderate degree of spatial and kinematic sub-structure and is commensurate with values measured in observed star-forming regions.

In most of our simulations we create star-forming regions containing $N_{\star}=100$ stars (as these are unlikely to contain many, or any, massive stars that produce photoionizing radiation that would preclude the formation of gas giant planets in our Solar system, R. B. Nicholson & R. J. Parker 2017; M. Patel et al. 2023). However, in one set of models we create simulations with $N_{\star}=300$, $N_{\star}=500$, and $N_{\star}=1000$ stars. Individual stellar masses are sampled from the Maschberger IMF, described in the form of the following probability density function:

$$P(M_{\star}) \propto \frac{M_{\star}}{\mu}^{-\alpha} \left(1 + \left(\frac{M_{\star}}{\mu}\right)^{1-\alpha}\right)^{-\beta},$$
 (1)

where M_{\star} is the star mass, α is the high-mass exponent ($\alpha=2.3$), β is the low-mass exponent ($\beta=1.4$), and μ is the scale parameter ($\mu=0.2$) (T. Maschberger 2013). Masses are constrained between 0.1 and $50\,\mathrm{M}_{\odot}$. Stellar discs are assumed to have a radius of 400 au, similar to the radius assumption made in R. J. Parker & C. Schoettler (2023), based on the estimated average disc radii in star-forming regions proximal to NGC 2264 (S. M. Andrews et al. 2013; L. A. Cieza et al. 2019). The lifetime of each disc is derived from an exponential probability density function with a mean lifetime of 2 Myr; at the end of this lifetime, SLR mass fractions are stored. Radioactive decay of SLRs within discs is modelled every time-step, and considered when determining the final SLR mass fraction after the disc has progressed to a protoplanetary system. While stars could

potentially form binary pairs the effect of binarity is not explicitly considered.

Much of the codebase of this project is shared with our previous paper (J. W. Eatson et al. 2024a), which contains a more detailed explanation of all the shared routines with this code.

2.2 Interloper enrichment

The main change between the simulation set-up in this paper and the model described in J. W. Eatson et al. (2024a) is the addition of routines to calculate the amount of SLR enrichment in discs due to AGB interlopers. Upon initialization of the simulation, a single AGB star is created in addition to the star-forming region, at a distance of x_i from the star-forming region and an initial velocity of v_i heading towards the centre of the simulation (approximately the barycentre of the star-forming region). A single AGB star is added to the N-body simulation, and thus can interact dynamically with the star-forming region. The AGB star's initial trajectory is towards the (0,0,0) co-ordinate of the simulation at an initial speed of v_i . Angled AGB trajectories are not simulated, instead we offset the AGB along the y simulation axis with the parameter y_i . Unless otherwise stated, the interloping star immediately enters the AGB phase at simulation start and begins depositing SLRs into the starforming region, however the start time of the AGB phase can be offset with the parameter τ_i . As SEBA does not support stars of mixed ages, stellar evolution of the AGB star itself is not considered, as such the mass of the interloping star may be higher than if the interloper were able to evolve, potentially influencing the dynamics of the starforming region as the interloper passes through it. Whilst this can result in differences in dynamics due to the changing mass of the AGB star, this was deemed an acceptable trade-off.

A series of lookup tables based on total SLR yields calculated in A. I. Karakas & M. Lugaro (2016) were formulated, the total yield was then spread over the lifetime of the AGB phase of the interloping star. Lookup tables for ²⁶Al and ⁶⁰Fe were produced; the injection of other SLRs such as 41Ca, 53Mn, 107Pd, and 182Hf were not modelled. This assumes that the ratio of mass-loss of SLRs from the interloper to the total wind mass-loss is constant over the AGB phase, but this is more accurate than assuming that the SLR mass-loss rate is constant and spread evenly over the AGB phase. The total yield was used to calculate the SLR fraction of the total mass-loss over the AGB phase, which was then used to estimate the SLR mass-loss rate at the stars current age based on the AGBs current mass-loss rate. Fig. 1 compares yield rates and total SLR yield for AGB stars of masses varying from 3 to $7 M_{\odot}$, and shows the SLR mass-loss rate steadily increases over time, and then rapidly surges at the end of the AGB phase. R. J. Parker & C. Schoettler (2023) details the results of changing interloper mass, while the higher mass cases produce similar levels of enrichment – $7 \, M_{\odot}$ producing the most – the lowmass 3 M_o case produces insufficient SLR quantities (this can also be seen in Fig. 1). For this paper, we use a single discrete interloper mass case of 7 M_{\infty}. By default, the interloper enters the AGB star immediately after the start of the simulation, but this can be offset at runtime, resulting in no enrichment until a defined time; this is referred to in our work as the interloper offset time, τ_i .

Disc SLR enrichment is calculated using the method described in J. W. Eatson et al. (2024a), though with the aforementioned AGB enrichment calculated as well. Similar to the model described in R. J. Parker & C. Schoettler (2023), we incorporate a cylindrical model of outflow from the interloper, as the flow is substantially slower than the Wolf–Rayet winds simulated in our previous paper. However, to account for deflection and potential trapping of the AGB by the star-

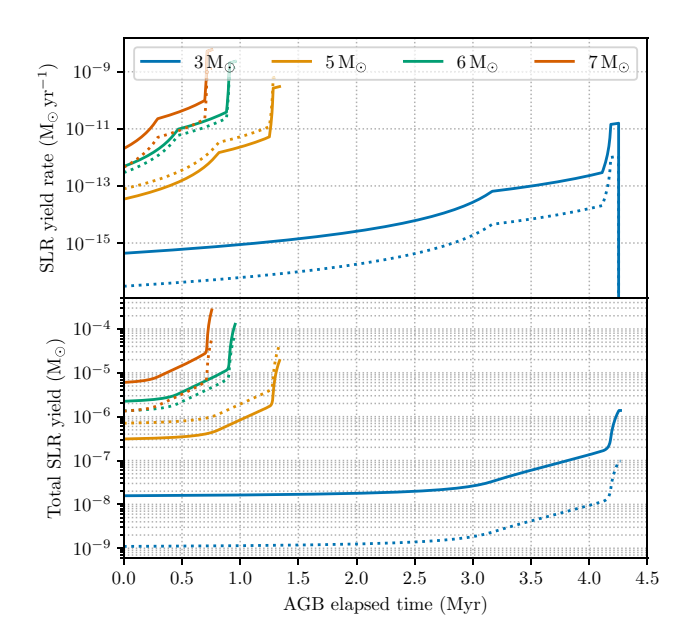


Figure 1. SLR yield rates and total yields for stars over their AGB phase, derived from the work in A. I. Karakas & M. Lugaro (2016). Higher mass stars have significantly shorter AGB phases, but have much higher emission rates and larger total yields.

forming region, we model the outflow region as a series of connected cylindrical segments. As the interloper moves through the simulation a new one is added every simulation time-step for the lifetime of the star, SLRs are deposited into the segment based on the current AGB SLR mass-loss rate, \dot{M}_{SLR} , such that

$$\mathbf{M}_{\mathrm{SLR,seg}} = \dot{\mathbf{M}}_{\mathrm{SLR}} \Delta t,\tag{2}$$

where Δt is the simulation time-step. The segment has a length equivalent to the distance travelled by the interloper between each time-step and a radius of 0.1 pc. After the *N*-body simulation has evolved at each time-step, every remaining disc is checked to see whether it is currently inside or has passed through a segment, with the fraction of the time-step that the star has intersected a cylinder segment defined as η_{int} .

The total mass sweep-up efficiency of the disc is calculated with the equation

$$\eta_{\rm sw} = \frac{r_{\rm disc}^2}{r_{\rm cyl}^2} \frac{d_{\rm trav}}{l_{\rm cyl}},\tag{3}$$

where $r_{\rm disc}$ is the disc radius, $d_{\rm trav}$ is the distance travelled within the cylinder by the approaching star during a time-step, and $r_{\rm cyl}$ is the cylinder radius. This is equivalent to the ratio of the volumes of two cylinders, the previously described segment and the straight-line path of the intersecting disc. The total disc sweep-up mass ($M_{\rm SLR,sw}$) can be then calculated with the formula

$$M_{SLR,sw} = \eta_{sw} \eta_{int} M_{SLR,seg}. \tag{4}$$

The amount of material removed from the segment is removed from the total SLR mass reserved of the segment, available SLR mass is reduced every time-step to account for radioactive decay processes. For a given simulation of a time-step of $10^4\,\rm yr$, this results in $\approx\!70$ discrete segments for a $7\,M_\odot$ star. Segments are not dispersed over time, as the dispersion time of this wind-blown region could vary significantly and would introduce a series of free parameters into the simulation; we therefore assume that the dispersion time is longer than the AGB time-scale of the interloping star.

This method expands on work by R. J. Parker & C. Schoettler (2023) by considering the trajectory of the AGB star, as well as a more accurate estimation of how discs interact with the AGB star via the changing trajectory of the AGB rather than a static cylinder. Future research could involve replacing the segmented cylinder with an SPH wind model, where density can be accurately sampled and effect of the AGB interloper moving through the local medium could be better simulated. Expansion of the cylinders over time to account for dispersion could also be performed.

The properties of the interloper can be varied at simulation start time, such parameters include the interloper mass (M_i) , the interlopers initial velocity towards the cluster (v_i) , and the interlopers initial position relative to the centre of the star-forming region along the x and y simulation axes $(x_i$ and $y_i)$. As with the previous paper (J. W. Eatson et al. 2024a), the radius of the star-forming region r_c , and total region population size, N_{\star} , can also be varied.

2.3 Parameter space explorations

The simulations performed in this paper can be broadly divided into multiple sets:

- (i) Set A: a broad parameter space search varying region radius, r_c , and interloper velocity, v_i .
- (ii) Set B: a series of simulations varying v_i and interloper AGB phase start time, τ_i .
- (iii) Set C: a series of simulations varying AGB initial position (x_i, y_i) , as well as v_i .
 - (iv) Set D: a series of simulations with larger stellar populations.

In order to ascertain which parameters of the star-forming region and interloper are influential, simulation set A is performed to determine the influence of the system parameters, as well as to test the interloper injection routines. Parameter combinations are repeated to rule out variation due to the structure and composition of the randomly generated clusters.

Once the ideal parameters for the interloper mass $(7\,{\rm M}_\odot)$ and region radius $(0.3\,{\rm pc})$ were established from the results of set A, we progressed to a finer parameter space search that varied v_i and τ_i . No repetition was performed on this set; instead τ_i was varied from 10^{-2} to $10\,{\rm Myr}$ and v_i was varied from 0.1 to $100\,{\rm km\,s^{-1}}$ in 32 logarithmically spaced steps each, leading to a total of 1024 discrete simulations. These simulations establish how influential the initial velocity and condition of the interloper is to the enrichment of a star-forming region.

Set C was designed to determine the effect of 'near-miss' interactions between the interloper and the star-forming region. The initial position of the interloper (x_i, y_i) was varied between -8 and 0 pc in the x simulation axis and 0 to 1 pc in the y simulation axis, where (0,0) is the initial centre of the star-forming region. The interloper immediately enters the AGB phase, unlike set B, and has an initial velocity of 1, 3, 10 or $30 \, \mathrm{km \, s^{-1}}$ on the x axis towards the star-forming region. x and y axis stepping is evenly spaced, with 64 discrete positions on the x axis and 8 discrete positions on the y axis, and similarly to set B, there is no repetition. Another sub-set of set C is also performed, where y_i is not varied, but the x_i range is increased to 25 pc, in order to observe enrichment due to more evolved, high-velocity interlopers. Whilst all previous simulation sets have a region population of $N_{\star} = 100$, set D differs by varying the population to either $N_{\star} = 300$, $N_{\star} = 500$, or $N_{\star} = 1000$.

Based on our results from set C the interloper for all simulations had an initial distance from the star-forming region of $x_i = 3.0 \,\mathrm{pc}$. Simulation repetition was performed, with larger simulations having

Table 1. A summary of the model sets performed in this paper, detailing which parameters are varied, by how much, whether simulations are repeated, as well as brief notes about the specifics of the simulation set are also included.

Set	Varied parameters	r _c range (pc)	v_i range (km s ⁻¹)	τ_i range (Myr)	N _⋆ range	Repetition	Notes
Set A	r_c, v_i	0.1, 0.3, 1.0	1, 3, 10, 30	0.0	100	Yes	Broad parameter search
Set B	τ_i , v_i	0.3	0.1-100	0.01-10	100	None	Logarithmically spaced search
Set C	x_i, y_i, v_i	0.3	1, 3, 10, 30	0	100	None	8 pc x_i range, 1 pc y_i range
Set C 2	x_i, v_i	0.3	0	0	100	None	25 pc x_i range
Set D	N_{\star}, v_i	0.3	0	0	100, 300, 500, 1000	Varies by N_{\star}	Changes population size

fewer repetitions in order for each parameter space set to have the same number of stars simulated, and to accommodate for increased computational complexity due to the increased number of stars. The interloper radius was also varied from 1 to $30\,\mathrm{km\,s^{-1}}$. An increased population will increase the total mass of the star-forming region, resulting in a greater escape velocity. This could enhance the likelihood of trapping lower velocity AGB stars. Table 1 is a concise reference of the differences between each simulation set.

3 RESULTS

3.1 Set A: initial simulations

For this simulation set, star-forming region radius, R_c , interloper mass, M_i , and interloper initial velocity, v_i , are varied in wide steps. Star-forming regions have $N_{\star} = 100$ stars, an initial radius of 0.1, 0.3, or 1.0 pc, which corresponds to a stellar density $(\bar{\rho})$ of $\sim 2 \times 10^4 \, \mathrm{pc^{-3}}$, $\sim 10^3 \, \mathrm{pc^{-3}}$ and $\sim 20 \, \mathrm{pc^{-3}}$, respectively. Interlopers are introduced into the simulation with a velocity of either 1, 3, 10 or 30 km s⁻¹ into a star-forming region of radius 0.1, 0.3, or 1.0 pc. The initial position of the interloper was 1 pc from the simulation centre, which is the approximate centre of the star-forming region as well. Parameter combinations were repeated 50 times to rule out random effects and variation due to initial cluster morphology, this is also used to calculate uncertainty for our results. This set acts as an initial parameter space exploration using our initial model, and is also used to verify whether the model is accurate by comparing it to previous work by R. J. Parker & C. Schoettler (2023).

Two useful values we will consider in our assessment are the ²⁶Al significant enrichment fraction, Z_{26Al,0.1SS}, and the Solar system ²⁶Al enrichment fraction, Z_{26Al,SS} (K. Thrane et al. 2006), which is the fraction of discs that undergo enrichment sufficient to affect planetesimal evolution, and the fraction of discs that undergo enrichment equivalent to the Solar system estimate for a given SLR. We define Z_{26Al,0.1SS} as a tenth of the early Solar ²⁶Al enrichment fraction due to simulations by T. Lichtenberg et al. (2019) as well as our previous results on planetesimal simulation (J. W. Eatson et al. 2024b). It was found that at around this amount, outgassing began to occur in a 100 km planetesimal. The effects of ⁶⁰Fe heating are less pronounced, with significant outgassing due to 60 Fe occurring at $Z_{60\text{Fe}}$ values that are two orders of magnitude higher than the higher Solar system enrichment estimate of ⁶⁰Fe (J. W. Eatson et al. 2024b). We consider two different values for quantifying the number of discs that have significant $Z_{60\text{Fe}}$ enrichment; the fraction of discs that exceed the low $(Z_{60\text{Fe}} > 10^{-8}; \text{H. Tang & N. Dauphas 2012})$ and high $(Z_{60\text{Fe}} > 10^{-6};$ R. K. Mishra et al. 2016) estimates for Solar system ⁶⁰Fe enrichment (see also D. L. Cook, B. S. Meyer & M. Schönbächler 2021; J. Kodolányi et al. 2022). These are labelled as $Z_{60\text{Fe,Lo}}$ and $Z_{60\text{Fe,Hi}}$ in Table 2, respectively. We also record the total mass of ²⁶Al and ⁶⁰Fe injected into discs in the star-forming region, M_{SLR.ini}, which we can compare with the total SLR mass-loss of a 7 M_{\odot} star. We calculate

these total mass-losses using the SLR yields in A. I. Karakas & M. Lugaro (2016), and were found to be $M_{26Al}\approx 2.7\times 10^{-4}\,M_{\odot}$ and $M_{60Fe}\approx 6.0\times 10^{-05}\,M_{\odot}$.

Table 2 contains the results for each combination of parameters performed in set A. We find that there is a wide variance of enrichment levels for discs, but there is a strong clustering correlation by parameter sub-set, as can be clearly seen in Fig. 2. With AGB enrichment discs can be enriched to values substantially exceeding Solar system levels, though the extremely highly enriched examples may not be possible, as we will later discuss. However, for more realistic parameters, early Solar levels of enrichment are indeed possible. We find that the cluster radius does not have an effect on the maximum amount of enrichment for a simulation sub-set. though it can drastically effect the number of stars undergoing enrichment, resulting in a total decrease in the fraction of discs enriched to any amount, Zen, of approximately an order of magnitude between the 0.1 and 1.0 pc. Influential enrichment levels are possible for extremely sparse star-forming regions, though this is much less likely. For successive simulation sets we adopted $r_c = 0.3 \,\mathrm{pc}$, similar to much of our previous work. The most important parameter explored was the initial velocity of the interloper, as the velocity increases Z_{en} increases, though there is a marked decrease in the number of stars that undergo significant amounts of enrichment as the velocity increases above $3 \mathrm{km} \, \mathrm{s}^{-1}$, $1 \mathrm{km} \, \mathrm{s}^{-1}$ cases have a reduced $Z_{\rm en}$. While counter-intuitive, this is due to taking ~ 1 Myr to reach the centre of the simulation, and thus would only interact with the outlying stars before ending the AGB phase. This elapsed time would also reduce the number of viable discs the AGB wind could interact with. In terms of the total SLR mass injected into every disc in the simulation, the slower simulations were found to inject far more material into the discs, with an efficiency of about 1 per cent, this decreased substantially as interloper velocity and r_c increase, though this still results in enrichment to levels that can influence the thermochemical evolution of subsequent planetesimals.

Compared to the Galactic velocity dispersion (30 km s⁻¹), 3 to 10 km s⁻¹ would constitute a relatively slow, 'walk-away' velocity star (C. Schoettler et al. 2020; C. Schoettler, R. J. Parker & J. de Bruijne 2022), but is within a reasonable value and coincides with the relative velocities of stars near to the Solar system. The 1 km s⁻¹ case, or stars lower than that, would be extremely unlikely. As such, our initial estimates suggest that AGB enrichment is a viable method of disc SLR enrichment, our subsequent simulation sets determine how sensitive this amount of enrichment is to the interlopers properties, as well as the initial conditions of the starforming region. It is also important to note that while ²⁶Al is a more important source of radioisotopic heating in the early Solar system, the interloper enrichment mechanism can produce ⁶⁰Fe enrichment in discs equivalent to early Solar system estimates. This level of ⁶⁰Fe enrichment was determined in our previous work to not be possible with Wolf-Rayet winds (J. W. Eatson et al. 2024a), and would require

Zone, Lo, the number enriched to the higher estimate for 60 Fe in the Solar system, Zone, Hi and the mass of 26 Al and 60 Fe injected into the discs, MocAl inj and Mone, inj, respectively. Enrichment is Pable 2. A collection of results from simulation set A, with the initial simulation parameters detailed. Uncertainties are based on running simulations with identical parameters 50 times. We show the simulation sufficient for volatile desiccation in planetesimals (T. Lichtenberg et al. 2019; J. W. Eatson et al. 2024b). Similarly, 60 Fe enrichment to the low Solar estimate is surprisingly common for faster interloper enrichment. tradius of the star-forming region rc, velocity of the interloper vi, the number of discs summed across all realizations of these simulations, Ndisctor. We then show the number of discs that have any enrichment, However, interlopers moving at or above the galactic velocity dispersion ($\approx 30\,\mathrm{km\,s^{-1}}$) are not conducive to enrichment, at least with an initial position of 1 pc from the centre of the star-forming region the number of discs enriched to the lower estimate for of $10 \, \text{km s}^{-1}$ case of simulations with $Z_{\rm en}$, the number of discs enriched to a tenth of the $^{26}{\rm Al}$ in the Solar system $Z_{26{\rm Al},0.15S}$, very dependent on the original velocity of the interloper, v_i , though even in the

Simulation sub-set	r_c	v_i km s ⁻¹	Ndisc,tot	$Z_{ m en}$	$Z_{26\mathrm{Al},0.1\mathrm{SS}}$	$Z_{26A1,SS}$	$Z_{ m 60Fe,Lo}$	$Z_{ m 60Fe, Hi}$	$M_{26A1,inj} \ M_{\odot}$	$ m M_{60Fe,inj}$ $ m M_{\odot}$
set-a-rc-0.1-inv-1.00	0.1	1.0	4841	0.29 ± 0.04	0.27 ± 0.04	0.24 ± 0.03	0.29 ± 0.04	0.29 ± 0.04	$(2.8 \pm 0.7) \times 10^{-6}$	$(8.7 \pm 2.2) \times 10^{-7}$
set-a-rc-0.1-inv-3.00	0.1	3.0	4840	0.64 ± 0.03	0.46 ± 0.03	0.23 ± 0.02	0.63 ± 0.03	0.39 ± 0.03	$(3.66 \pm 0.35) \times 10^{-8}$	$(1.17 \pm 0.13) \times 10^{-8}$
set-a-rc-0.1-inv-10.0	0.1	10.0	4844	0.81 ± 0.01	0.17 ± 0.01	0.0002 ± 0.0002	0.70 ± 0.02	0.0004 ± 0.0003	$(2.10 \pm 0.13) \times 10^{-9}$	$(6.0 \pm 0.4) \times 10^{-10}$
set-a-rc-0.1-inv-30.0	0.1	30.0	4872	0.890 ± 0.008	0.008 ± 0.002	0.0	0.49 ± 0.02	0.0	$(4.88 \pm 0.22) \times 10^{-10}$	$(1.30 \pm 0.07) \times 10^{-10}$
set-a-rc-0.3-inv-1.00	0.3	1.0	4839	0.17 ± 0.02	0.14 ± 0.01	0.11 ± 0.01	0.17 ± 0.02	0.16 ± 0.01	$(5.7 \pm 0.7) \times 10^{-7}$	$(1.90 \pm 0.26) \times 10^{-7}$
set-a-rc-0.3-inv-3.00	0.3	3.0	4847	0.37 ± 0.02	0.22 ± 0.01	0.075 ± 0.005	0.37 ± 0.02	0.152 ± 0.009	$(1.05 \pm 0.07) \times 10^{-8}$	$(3.8 \pm 0.4) \times 10^{-9}$
set-a-rc-0.3-inv-10.0	0.3	10.0	4867	0.47 ± 0.01	0.047 ± 0.003	0.0	0.38 ± 0.01	0.0002 ± 0.0002	$(6.69 \pm 0.23) \times 10^{-10}$	$(2.17 \pm 0.09) \times 10^{-10}$
set-a-rc-0.3-inv-30.0	0.3	30.0	4855	0.48 ± 0.01	0.0004 ± 0.0003	0.0	0.188 ± 0.007	0.0	$(1.53 \pm 0.05) \times 10^{-10}$	$(4.56 \pm 0.14) \times 10^{-11}$
set-a-rc-1.0-inv-1.00	1.0	1.0	4846	0.026 ± 0.003	0.019 ± 0.002	0.011 ± 0.002	0.026 ± 0.003	0.021 ± 0.002	$(3.9 \pm 1.0) \times 10^{-8}$	$(1.41 \pm 0.31) \times 10^{-8}$
set-a-rc-1.0-inv-3.00	1.0	3.0	4845	0.081 ± 0.004	0.039 ± 0.003	0.014 ± 0.002	0.078 ± 0.004	0.029 ± 0.002	$(2.1 \pm 0.4) \times 10^{-9}$	$(1.07 \pm 0.34) \times 10^{-9}$
set-a-rc-1.0-inv-10.0	1.0	10.0	4838	0.096 ± 0.005	0.006 ± 0.001	0.0	0.075 ± 0.004	0.0	$(9.5 \pm 0.6) \times 10^{-11}$	$(3.58 \pm 0.22) \times 10^{-11}$
set-a-rc-1.0-inv-30.0	1.0	30.0	4862	0.074 ± 0.004	0.0	0.0	0.025 ± 0.002	0.0	$(1.56 \pm 0.09) \times 10^{-11}$	$(5.70 \pm 0.35) \times 10^{-12}$

supernovae, which would destroy the gas within the discs (M. Patel et al. 2023), resulting in a lack of gas giant planets in the planetary system(s).

3.2 Set B: AGB time offset

In this set of simulations, the variable parameters are the initial interloper velocity, v_i and the interloper time offset, τ_i . v_i is logarithmically spaced varying from 0.1 to 100 km s⁻¹, τ_i was similarly spaced between 0.01 to 10 Myr. The interloper was placed at a distance of 1 pc from the centre of the star-forming region, and the region has a radius of $r_c = 0.3$ pc. Fig. 3 shows the enrichment fractions for each simulation in this set, in ideal conditions the number of discs in a simulation that undergo near-Solar enrichment can exceed 30 per cent, with some consistency. Whilst this puts the Solar system in the upper limit of disc enrichment if our results in set A are also considered, this suggests that if AGBs encounter discs at 'walk-away' speeds - below the velocity dispersion of the Milky Way - ²⁶Al enrichment would be an important driving force in planetesimal formation (T. Lichtenberg et al. 2019; J. W. Eatson et al. 2024b). Broadly speaking, significant disc enrichment becomes common between 1 and 10 km s⁻¹, with a relatively sharp cutoff above 10 km s⁻¹. While the high velocity of the interloper is a contributing factor to this lack of enriched discs - as SLRs are spread more sparsely over a wider area – another reason would be that the interloper simply passes by the cluster before AGB outflow is heightened, a few hundred thousand years into its lifespan. This can be observed in the lower velocity simulations with a higher value for τ_i , and is investigated further in set C by varying the interlopers initial distance to the cluster instead. Furthermore, as the disc population halves every 2 Myr, this can also reduce the enriched disc population. Fig. 4 shows distances from AGB interlopers to their nearest cluster stars for a sample of the set B data where $\tau_i = 0.01 \text{Myr}$. In the case of very low velocity interlopers, the interloper does not continue its progress away from the star-forming region, instead becoming 'trapped'. This is to be expected, as these velocities are below the regions escape velocity, however, this leads to the interloper interacting with nearly every disc in the region, and would also lead to multiple interaction occurrences for individual discs. The probability of this occurring is potentially low, however, but would lead to extremely enriched discs in star-forming regions. Such a study is beyond the scope of this paper, but would deem investigation if 'trapped' interlopers were found in observed regions.

3.3 Set C: AGB distance offset

In order to verify where significant enrichment of discs is possible via higher velocity interlopers, in this set we start the interloper at a varying distance to the star-forming region, from -8 to 0 pc. We also vary the y axis offset from 0 to 1 pc – or 3 times the region radius - to determine the effect on enrichment due to 'near misses', where the interloper does not directly run through the centre of mass of the star-forming region. We also vary the velocity of the AGB from 1 to 30 km s⁻¹. Fig. 5 clearly shows again that 10 km s⁻¹ is a very viable velocity for disc enrichment, and enrichment is not significantly influenced by initial distance, so long as the interloper encounters the cluster after it has had time to reach a point where SLR production is increased compared to the start of the AGB phase. In general, in fact, velocity increases, the parameter space where disc enrichment is viable spreads out. The average fraction of suitably enriched discs does also decrease as velocity increases, due to a sparser field of SLRs for the discs to sweep up. However, by 30 km s⁻¹ disc enrichment to

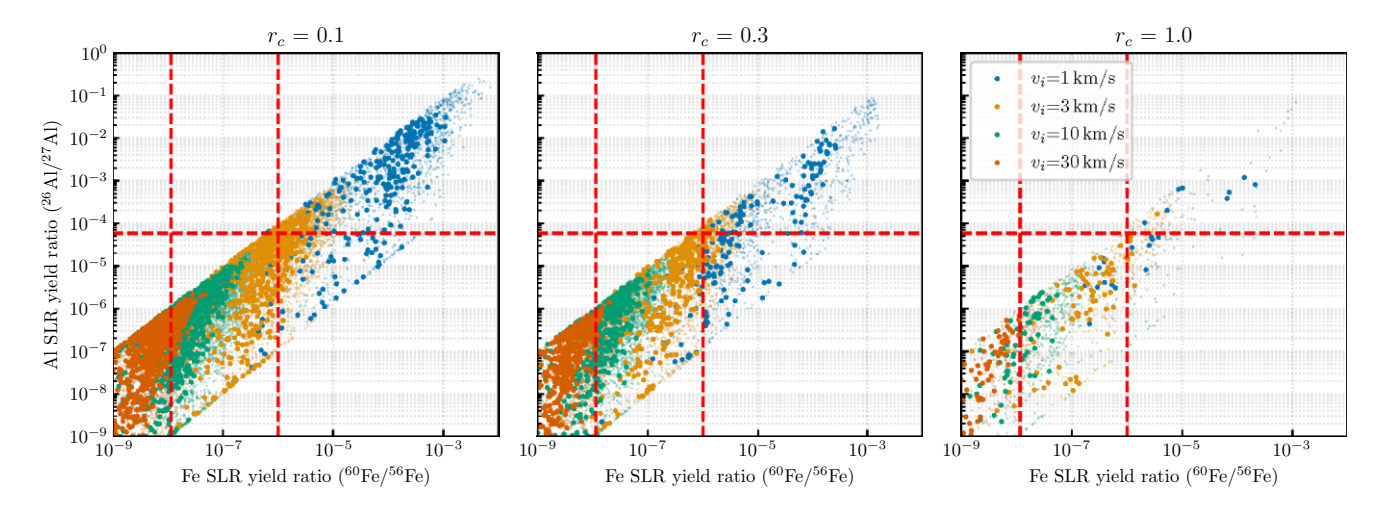


Figure 2. A comparison of 26 Al and 60 Fe enrichment for set A simulations, split by r_c . Opaque, larger markers represent discs with a host star between 0.5 and 1.5 M $_{\odot}$. Discs with Solar system levels with a Solar-like host star are possible, though infrequent. Dashed lines represent estimated Solar system formation levels of enrichment based on observational data. Enrichment amount does not vary considerably as r_c is varied, though the probability of the discs undergoing high levels of enrichment decreases significantly. There is a clear inverse relationship between v_i and enrichment of either isotope.

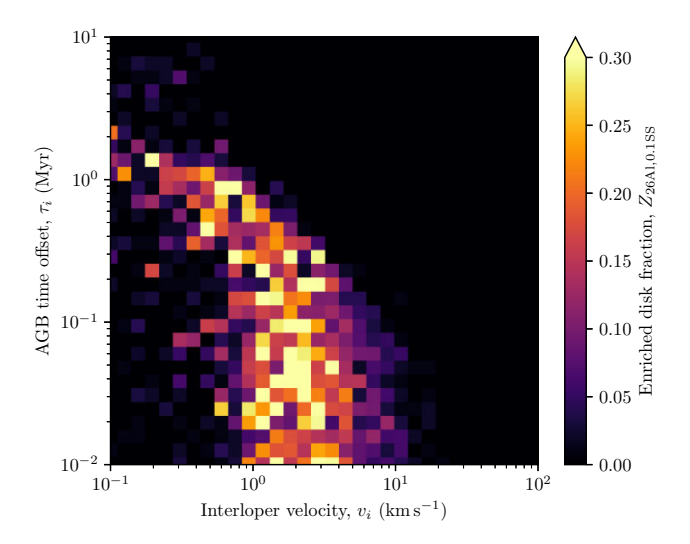


Figure 3. Enrichment fractions for each simulation in the B set. There is a strong dependency on interloper velocity and yield, with a significant reduction in enrichment as the initial interloper velocity exceeds $10\,\mathrm{km\,s^{-1}}$. Whilst there is also an inverse relationship with enrichment and interloper AGB phase offset time, this is largely due to a lack of viable protoplanetary discs.

sufficient levels for thermochemical evolution does still occur, just in numbers. This is due to the resulting cloud of SLRs from the wind outflow being too diffuse, and as such sweep-up per unit time becomes too low.

Fig. 6 contains data from a sub-set of set C where y_i was not varied, but x_i was varied out to 25 pc instead, with steps every 0.1 pc. This was performed in order to better determine the variability between simulations and to also determine if 30 km s^{-1} cases could produce a large population of discs. We found that 30 km s^{-1} could in fact produce lower, but still prominent ($\sim 10 \text{ per cent}$) fractions of enriched discs. This enrichment fraction as a function of distance is similarly flat beyond a minimum value like the 10 km s^{-1} case in Fig. 5, though with a more prominent peak. Filtering the sub-set down to discs with Solar-like host stars and comparing isotopic enrichment

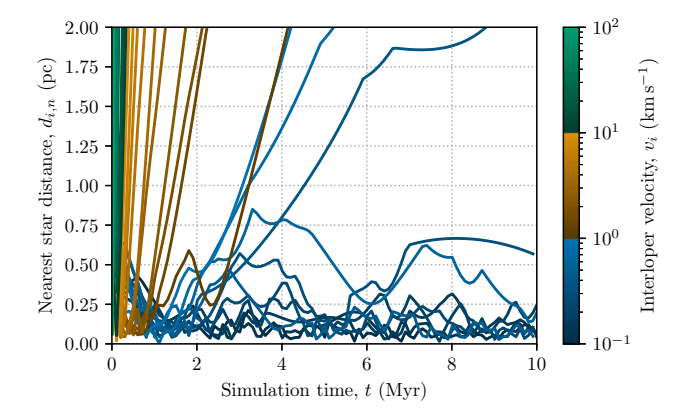


Figure 4. Interloper distance from the nearest star over time for simulations where the interloper enters the AGB phase immediately after the start of the simulation. Most interlopers do not become trapped in the star-forming region.

instead (Fig. 7), we find that very high levels of enrichment can occur, to the point where ^{60}Fe enrichment could be influential in devolatilization (J. W. Eatson et al. 2024b). The results of sets B and C suggest that the interloper being in the latter part of its AGB phase is extremely important to disc enrichment, with interlopers with velocities at or above the galactic velocity dispersion ($\sim 30\,\text{km}\,\text{s}^{-1}$) able to enrich discs to levels where substantial desiccation can occur.

3.4 Set D: larger simulations

For the final set of simulations in this paper the intent was to determine how star-forming regions with higher densities with larger populations would affect disc enrichment. In this set, simulations with a total star-forming region population of 100, 300, 500 or 1000 stars were introduced to an interloper of a velocity of either 1, 3, 10, or 30 km s⁻¹. The interloper placed at a distance of 3 pc from the cluster initially. Repetition was performed for each parameter space combination, but the number of repetitions were scaled with the population size in order to ensure approximately the

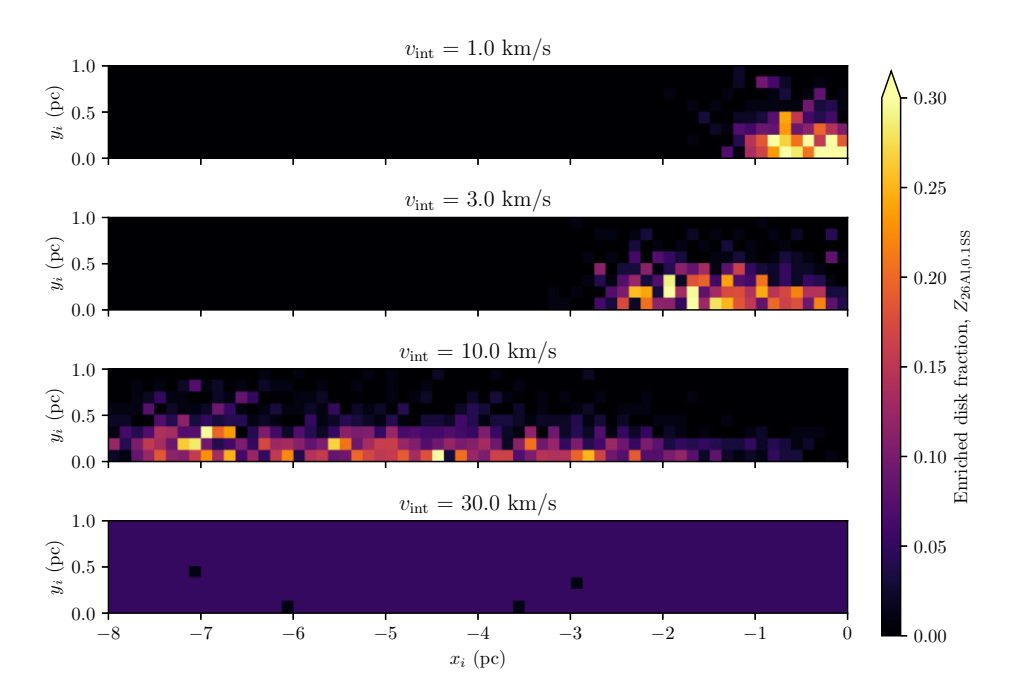


Figure 5. Comparison of enrichment in simulations where interloper x_i and y_i offset are changed. Results are separated by initial interloper velocity. The $10 \,\mathrm{km} \,\mathrm{s}^{-1}$ case consistently produces some highly enriched discs, as long as the interloper is given some time to evolve before it interacts with the star-forming region.

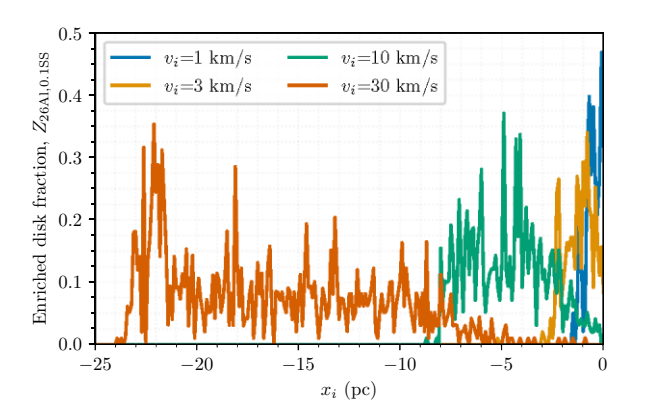


Figure 6. Comparison of 26 Al enrichment in simulations where x_i and v_i are changed. An expanded and higher density x_i parameter space is used compared to the data in Fig. 5, we find that lowered, but still viable levels of Solar-like 26 Al enrichment occur in the 30 km s⁻¹ case, suggesting that main influences on enrichment are the progression of the interloper into the AGB phase as well as the interlopers velocity.

same number of total discs for each parameter space combination (100-star simulations were repeated 60 times, 300-star were repeated 20 times, 500-star repeated 12 times, and 1000-star simulations repeated 6 times). There is some fluctuation in the total number of discs between sub-sets, this is due to varying numbers of high-mass stars between simulations.

Table 3 details the averaged results of the set D simulations. Enrichment quantity is found to vary due to velocity, as observed in previous simulation sets, what is notable is that there is not a significant difference in enrichment due to population size. This is further expounded upon by Fig. 8, where we can see that the only major difference between each population bin is the population of discs with Solar-like parent stars, due to the increased cluster

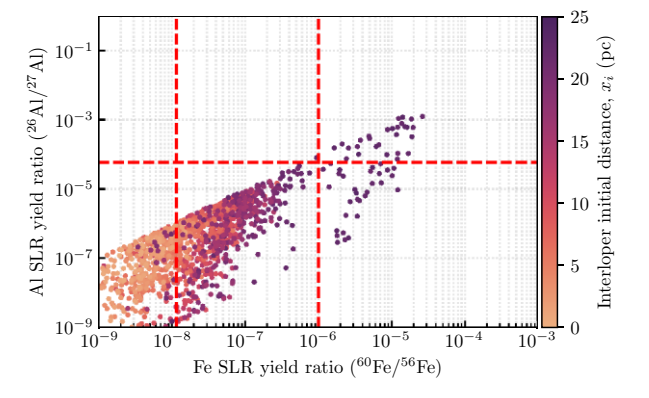


Figure 7. A comparison of isotopic ratios for all discs with Solar-like parent stars in the Fig. 6 sub-set where $v_i = 30 \, \mathrm{km \, s^{-1}}$. A small number of discs have significantly elevated SLR enrichment, to the point where even 60 Fe would be an important desiccant, though 26 Al would still be the dominant heating source in eventual planetesimal evolution.

population. In the 1000-star sub-set, we see that $v_i = 1 \,\mathrm{km}\,\mathrm{s}^{-1}$ enriched discs are present, despite the greater distance needed to travel from the start of the simulation. This can be attributed to a larger number of stars at the periphery of the cluster, as well as the increased gravitational attraction of the more massive cluster. Fig. 9 shows the distance from the interloper to the nearest cluster star as a function of time, binned by velocity, we see that in the more massive cluster cases the interloper 'trapping' seen in Fig. 4 also occurs. However, this would not affect the results of this set significantly as the limiting factor is the time required for the interloper to intersect the cluster. Overall, this further shows that interloper timing and velocity are the most important factors in causing efficient SLR enrichment, and an increased star-forming

Table 3. A table of the averaged results for each sub-set of the simulations in set D, similar to Table 2. There is a small correlation on Solar system level enrichment probability and star count, however, this is relatively minor.

Simulation name	N _*	$v_i \\ \mathrm{km}\mathrm{s}^{-1}$	$N_{ m disc,tot}$	$Z_{ m en}$	$Z_{26Al,0.1SS}$	$Z_{26Al,SS}$	$Z_{60{ m Fe,Lo}}$	$Z_{60{ m Fe,Hi}}$	M26A1,inj M⊙	$ m M_{60Fe,inj}$ $ m M_{\odot}$
set-d-v-1.00-ns-0100	100	1.0	5857	0.0012 ± 0.0004	0.0008 ± 0.0004	0.0005 ± 0.0003	0.0012 ± 0.0004	0.0012 ± 0.0004	$(1.2 \pm 0.9) \times 10^{-9}$	$(9 \pm 5) \times 10^{-10}$
set-d-v-3.00-ns-0100	100	3.0	5825	0.26 ± 0.01	0.194 ± 0.009	0.120 ± 0.008	0.26 ± 0.01	0.20 ± 0.01	$(1.66 \pm 0.31) \times 10^{-7}$	$(5.9 \pm 1.0) \times 10^{-8}$
set-d-v-10.0-ns-0100	100	10.0	5826	0.42 ± 0.01	0.087 ± 0.004	0.0	0.38 ± 0.01	0.0008 ± 0.0004	$(1.19 \pm 0.04) \times 10^{-9}$	$(3.81 \pm 0.15) \times 10^{-10}$
set-d-v-30.0-ns-0100	100	30.0	5824	0.48 ± 0.01	0.0017 ± 0.0005	0.0	0.23 ± 0.01	0.0	$(1.86 \pm 0.07) \times 10^{-10}$	$(5.52 \pm 0.24) \times 10^{-11}$
set-d-v-1.00-ns-0300	300	1.0	5825	0.0017 ± 0.0009	0.0012 ± 0.0006	0.0007 ± 0.0003	0.0017 ± 0.0009	0.0014 ± 0.0007	$(6 \pm 4) \times 10^{-9}$	$(5.1 \pm 3.0) \times 10^{-9}$
set-d-v-3.00-ns-0300	300	3.0	5812	0.35 ± 0.03	0.27 ± 0.03	0.16 ± 0.02	0.35 ± 0.03	0.28 ± 0.03	$(3.9 \pm 1.0) \times 10^{-7}$	$(1.8 \pm 0.6) \times 10^{-7}$
set-d-v-10.0-ns-0300	300	10.0	5807	0.48 ± 0.02	0.117 ± 0.007	0.0017 ± 0.0006	0.44 ± 0.02	0.0033 ± 0.0008	$(4.68 \pm 0.30) \times 10^{-9}$	$(1.64 \pm 0.12) \times 10^{-9}$
set-d-v-30.0-ns-0300	300	30.0	5802	0.55 ± 0.02	0.003 ± 0.001	0.0	0.29 ± 0.02	0.0	$(7.7 \pm 0.5) \times 10^{-10}$	$(2.39 \pm 0.18) \times 10^{-10}$
set-d-v-1.00-ns-0500	500	1.0	5824	0.002 ± 0.002	0.001 ± 0.001	0.0007 ± 0.0007	0.002 ± 0.002	0.002 ± 0.002	$(1.3 \pm 1.2) \times 10^{-9}$	$(4 \pm 4) \times 10^{-9}$
set-d-v-3.00-ns-0500	500	3.0	5824	0.35 ± 0.04	0.26 ± 0.03	0.15 ± 0.02	0.35 ± 0.04	0.27 ± 0.04	$(3.5 \pm 0.6) \times 10^{-7}$	$(1.4 \pm 0.4) \times 10^{-7}$
set-d-v-10.0-ns-0500	200	10.0	5815	0.48 ± 0.03	0.121 ± 0.009	0.0002 ± 0.0002	0.45 ± 0.03	0.004 ± 0.002	$(8.1 \pm 0.6) \times 10^{-9}$	$(3.0 \pm 0.4) \times 10^{-9}$
set-d-v-30.0-ns-0500	200	30.0	5814	0.55 ± 0.02	0.0041 ± 0.0009	0.0	0.30 ± 0.02	0.0	$(1.30 \pm 0.08) \times 10^{-9}$	$(4.14 \pm 0.33) \times 10^{-10}$
set-d-v-1.00-ns-1000	1000	1.0	5826	0.03 ± 0.03	0.03 ± 0.02	0.02 ± 0.02	0.03 ± 0.03	0.03 ± 0.03	$(4 \pm 4) \times 10^{-7}$	$(5 \pm 4) \times 10^{-7}$
set-d-v-3.00-ns-1000	1000	3.0	5836	0.51 ± 0.03	0.40 ± 0.03	0.23 ± 0.03	0.51 ± 0.03	0.42 ± 0.04	$(5.9 \pm 0.7) \times 10^{-7}$	$(2.5 \pm 0.5) \times 10^{-7}$
set-d-v-10.0-ns-1000	1000	10.0	5830	0.56 ± 0.03	0.16 ± 0.02	0.003 ± 0.001	0.54 ± 0.03	0.012 ± 0.005	$(2.34 \pm 0.29) \times 10^{-8}$	$(9.0 \pm 1.3) \times 10^{-9}$
set-d-v-30.0-ns-1000	1000	30.0	5814	0.64 ± 0.02	0.007 ± 0.002	0.0	0.41 ± 0.04	0.0	$(3.8 \pm 0.4) \times 10^{-9}$	$(1.34 \pm 0.20) \times 10^{-9}$

region population size does not significantly affect enrichment amount.

4 DISCUSSION

Based on our results we have determined that an interloping AGB star is an effective method of SLR enrichment, especially for the SLR ⁶⁰Fe. Whilst Wolf–Rayet star winds can produce the amount of ²⁶Al enrichment present in the early Solar system, the disc disruption from these massive stars (R. B. Nicholson et al. 2019; E. C. Daffern-Powell & R. J. Parker 2022; M. Patel et al. 2023) and the long time-scales to attain supernovae enrichment in ⁶⁰Fe (M. Limongi & A. Chieffi 2018; T. Ertl et al. 2020) would likely preclude the formation of giant planets (though WR winds and/or supernovae could still be a viable SLR source for planetary systems devoid of gas giants).

We have shown that the delivery of SLRs from AGB stars is capable of explaining the observed abundances in the early Solar system, whilst also preserving the protoplanetary disc as the AGB stars have much slower winds and limited far-ultraviolet (FUV) flux. Our simulations produce higher-than-Solar ²⁶Al concentrations, and frequently produces ⁶⁰Fe enrichment above the higher estimate value. Whilst interlopers can cause significant amounts of enrichment, the amount of enrichment is dependent on a number of parameters. Principally, interloper velocity and ensuring the interloping AGB star is experiencing a high rate of mass-loss as it passes through the starforming region are the most crucial variables observed. In our earlier simulations enrichment was highly stratified by velocity, this was due to not adjusting the interlopers initial distance, x_i , from the cluster. From these simulations we observed that above $v_i = 10 \,\mathrm{km}\,\mathrm{s}^{-1}$ enrichment to Solar system levels becomes unlikely, though this is still within the expected range of relative velocities between nearby objects in the galaxy. However, our later simulations which varied x_i and y_i significantly show that with a large enough initial distance to the star-forming region, large numbers of enriched discs can be produced again, even with interloper velocities approaching 30 ${\rm km}\,{\rm s}^{-1}$. We can infer from this that the initial time before intersection is more important, and that in the case of higher velocity interlopers, the amount of discs that undergo significant enrichment is actually quite insensitive to the initial interloper position - provided that it has reached a later period of the AGB phase where mass-loss rates are higher. With a suitable initial distance or time before interaction, even 'runaway' interlopers ($v_i > 30 \,\mathrm{km \, s^{-1}}$) can significantly enrich discs in star-forming regions.

The initial mass or population of the cluster does not significantly affect results, aside from gravitationally, where AGBs are accelerated towards the star-forming region at a greater rate if the mass of the star-forming region is higher. In some of our higher mass star-forming regions the interloping AGB star can be trapped, and while this does cause increased amounts of enrichment, the higher mass regions are also more likely to contain massive stars (R. J. Parker & S. P. Goodwin 2007; R. B. Nicholson & R. J. Parker 2017) which would destroy the protoplanetary discs (F. Concha-Ramírez et al. 2019; R. B. Nicholson et al. 2019). In order to trap AGB stars in low-mass ($N_{\star}=100$) star-forming regions, interloper velocities $<1\,\mathrm{km\,s^{-1}}$ are required.

Whilst AGB interlopers could be a potential mechanism of SLR enrichment, a few outlying questions remain. In particular, the probability of these interloping events even occurring has not been ascertained, a single example exists in literature, while there are other potential interloper candidates, no wide-scale survey for these interlopers has been performed. We also observe that 'near-misses' from interlopers, which come within $2 \, r_c$ of the star-forming region

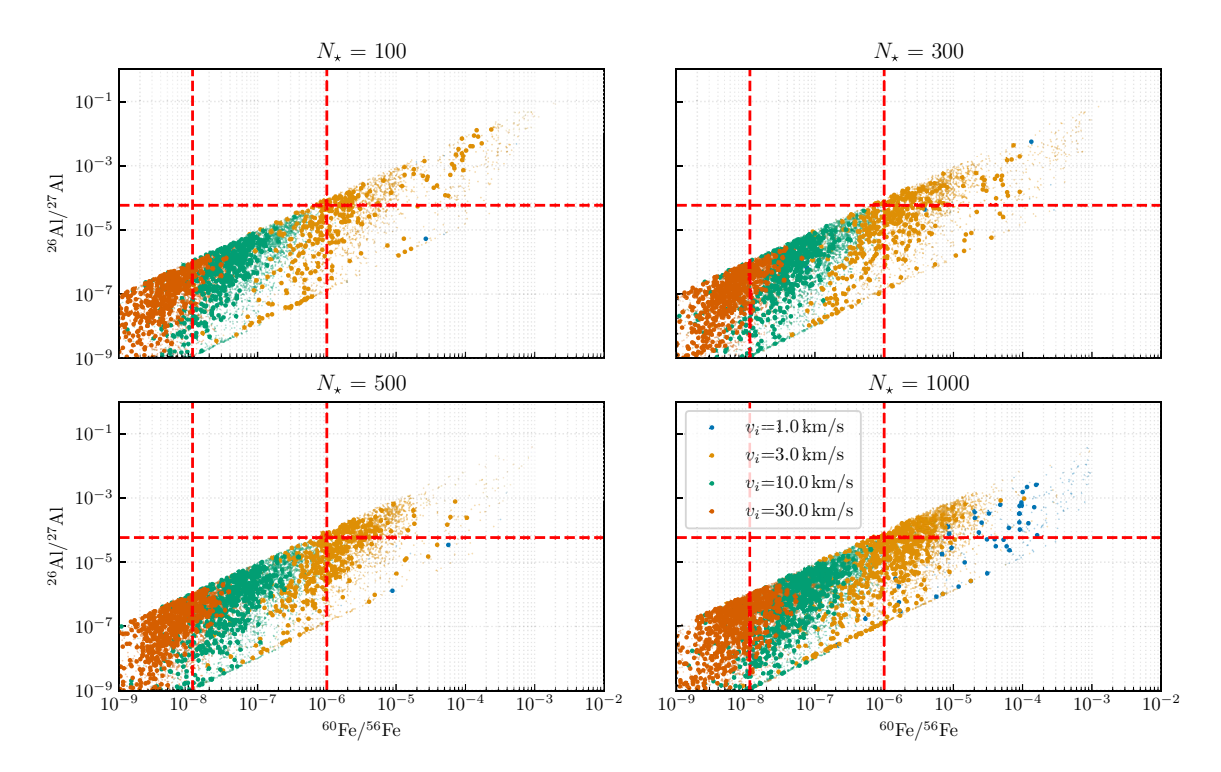


Figure 8. A comparison of 26 Al and 60 Fe enrichment for set D simulations, split by N_{\star} . We see that there is a minor improvement in enrichment in larger star-forming regions in general, however, enrichment is still very velocity dependent, and high-velocity 30 km s^{-1} interlopers do not enrich to Solar system levels.

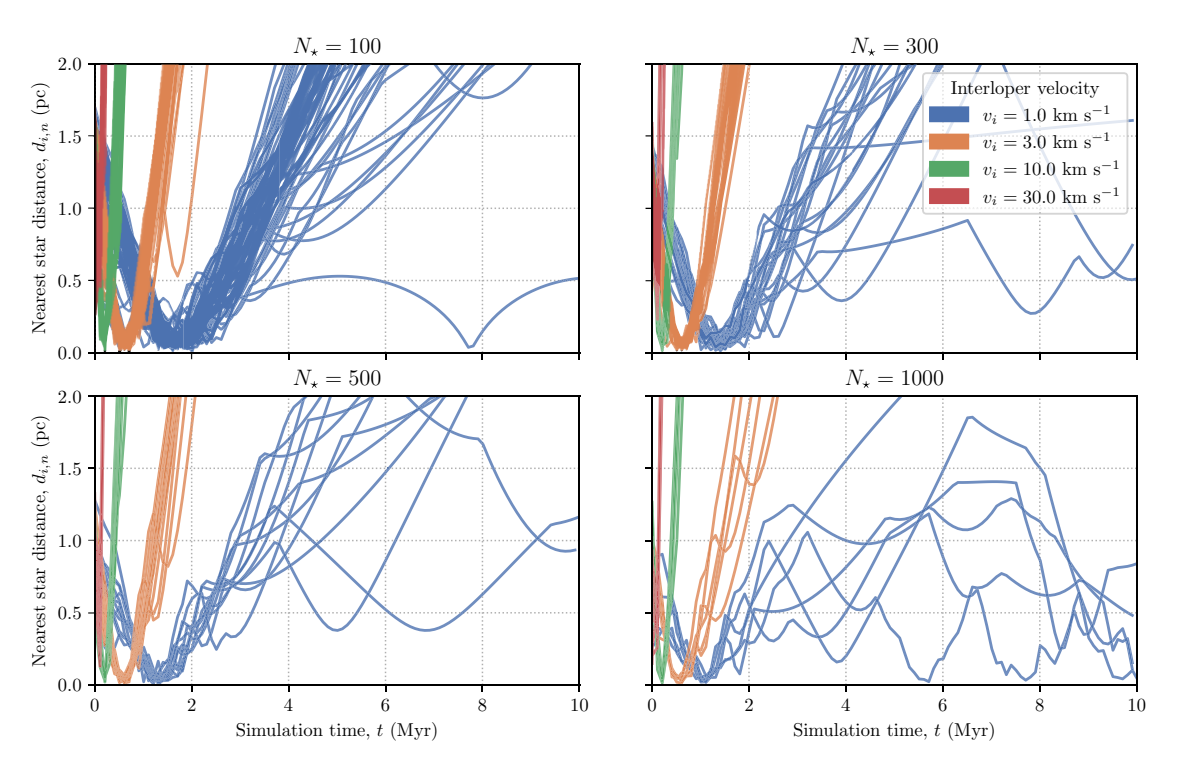


Figure 9. A comparison of the distance between the interloper and the nearest star for the simulations in set D over time, separated by interloper velocity, v_i . This is a similar plot to Fig. 4.

can still cause enrichment, as such, as long as the interloper passes through or near the star-forming region, enrichment can occur. This increases the probability of successful enrichment, as the star does not have to pass directly through the star-forming region. Future data

releases from *Gaia* could provide additional examples of interlopers, and may also reveal the presence of trapped AGB interlopers. An outlying concern with our current model are the presence of some free parameters in our simulations. Using a large – though still probable

– disc size would result in larger enrichments amounts; discs on the order of 100 au would result in an approximately order-of-magnitude change, still enough for a few highly enriched discs. Uncertainties also exist in the efficiency of core-produced SLRs such as $^{60}{\rm Fe}$ being transferred to the winds, though this would reduce $^{60}{\rm Fe}$ enrichment closer to the H. Tang & N. Dauphas (2012) low-estimate value of $Z_{60{\rm Fe}}=10^{-8}$. Additionally, modelling dissipation of the AGB wind over time would result in a lower amount of enrichment, while SLR decay within the 'tunnel' of the AGBs previous path is accounted for, expansion of the region as the wind outflows would decrease the density of the region, resulting in a lower rate of absorption of material. The latter issue could be addressed in a subsequent model that utilizes a smoothed particle hydrodynamics (SPH)-based outflow model from the AGB star, and would not require the use of interaction regions.

5 CONCLUSIONS

In this paper, we performed a large parameter space search using an *N*-body model to explore how the combined initial conditions of a star-forming region and interception properties of an interloping AGB star affect the enrichment of protoplanetary discs with shortlived radioisotopes. Our conclusions are the following:

- (i) We found that interloping AGB stars offer an abundant source of both ²⁶Al and ⁶⁰Fe, and can enrich multiple discs in a low-mass star-forming region to Solar system amounts in a short period of time (several Myr), absent of locally produced massive stars and supernovae.
- (ii) Interloper enrichment is sensitive to certain parameters, in particular the time at which the AGB begins interacting with the star-forming region, as well as its initial velocity.
- (iii) It appears that in the case of low-velocity 'walkaway' interlopers, the interloper can be captured by the star-forming region, rather than simply passing through it. Whilst this event produces marginally more enrichment from the AGB, it is less likely, and is not a requirement for high (Solar system-like) levels of enrichment.

Future work should focus on determining the overall probability of star-forming regions undergoing an interloper encounter. In addition, observational searches for further interloping (and/or trapped AGB stars) in star-forming regions would help determine the likelihood of Solar system (and other planetary system) enrichment from AGB stars. AGB stars, being the primary source of interstellar dust in the galaxy, have an outsized impact on the interstellar medium, and their being responsible for another facet of planetary evolution is well worth further investigation.

ACKNOWLEDGEMENTS

JWE and RJP acknowledge funding from the Royal Society, in the form of a Dorothy Hodgkin research fellowship award to RJP.

DATA AVAILABILITY

The data underlying this article will be shared on reasonable request to the corresponding author.

REFERENCES

André P., Di Francesco J., Ward-Thompson D., Inutsuka S.-I., Pudritz R. E., Pineda J. E., 2014, in Beuther H., Klessen R. S., Dullemond C. P.,

Henning T., eds, Protostars and Planets VI. Univ. Arizona Press, Tucson, p. 27

Andrews S. M., Rosenfeld K. A., Kraus A. L., Wilner D. J., 2013, ApJ, 771, 129

Arnould M., Paulus G., Meynet G., 1997, A&A, 321, 452

Barnes J., Hut P., 1986, Nature, 324, 446

Bate M. R., 2012, MNRAS, 419, 3115

Busso M., Gallino R., Wasserburg G. J., 1999, ARA&A, 37, 239

Cartwright A., Whitworth A. P., 2004, MNRAS, 348, 589

Cieza L. A. et al., 2019, MNRAS, 482, 698

Coleman G. A. L., Haworth T. J., Qiao L., 2025, MNRAS, 539, 1190

Concha-Ramírez F., Wilhelm M. J. C., Portegies Zwart S., Haworth T. J., 2019, MNRAS, 490, 5678

Cook D. L., Meyer B. S., Schönbächler M., 2021, ApJ, 917, 59

Curry A., Bonsor A., Lichtenberg T., Shorttle O., 2022, MNRAS, 515, 395

Daffern-Powell E. C., Parker R. J., 2020, MNRAS, 493, 4925

Daffern-Powell E. C., Parker R. J., 2022, MNRAS, 517, 2103

Davis A. M., 2022, Ann. Rev. Nucl. Part. Sci., 72, 339

Desch S. J., Young E. D., Dunham E. T., Fujimoto Y., Dunlap D. R., 2022,arXiv:preprint (arXiv.2203.11169)

Eatson J. W., Parker R. J., Lichtenberg T., 2024a, ApJ, 977, 13

Eatson J. W., Lichtenberg T., Parker R. J., Gerya T. V., 2024b, MNRAS, 528, 6619

Ertl T., Woosley S. E., Sukhbold T., Janka H. T., 2020, ApJ, 890, 51

Girichidis P., Federrath C., Allison R., Banerjee R., Klessen R. S., 2012, MNRAS, 420, 3264

Gomez M., Hartmann L., Kenyon S. J., Hewitt R., 1993, AJ, 105, 1927

Goodwin S. P., Whitworth A. P., 2004, A&A, 413, 929

Gounelle M., 2015, A&A, 582, A26

Gounelle M., Meibom A., 2008, ApJ, 680, 781

Gounelle M., Meynet G., 2012, A&A, 545, A4

Hacar A., Tafalla M., Alves J., 2017, A&A, 606, A123

Hirschmann M. M., Bergin E. A., Blake G. A., Ciesla F. J., Li J., 2021, PNAS, 118, e2026779118

Karakas A. I., 2014, MNRAS, 445, 347

Karakas A. I., Lugaro M., 2016, ApJ, 825, 26

Kastner J. H., Myers P. C., 1994, ApJ, 421, 605

Kodolányi J., Hoppe P., Vollmer C., Berndt J., Müller M., 2022, ApJ, 940, 95

Lichtenberg T., Parker R. J., Meyer M. R., 2016, MNRAS, 462, 3979

Lichtenberg T., Golabek G. J., Burn R., Meyer M. R., Alibert Y., Gerya T. V., Mordasini C., 2019, Nat. Astron., 3, 307

Limongi M., Chieffi A., 2006, ApJ, 647, 483

Limongi M., Chieffi A., 2018, ApJS, 237, 13

Lugaro M., Karakas A. I., 2008, New Astron. Rev., 52, 416

Lugaro M., Ott U., Kereszturi A., 2018, Prog. Part. Nucl. Phys., 102, 1

Maschberger T., 2013, MNRAS, 429, 1725

Mishra R. K., Marhas K. K., Sameer, 2016, Earth Planet. Sci. Lett., 436, 71

Nicholson R. B., Parker R. J., 2017, MNRAS, 464, 4318

Nicholson R. B., Parker R. J., Church R. P., Davies M. B., Fearon N. M., Walton S. R. J., 2019, MNRAS, 485, 4893

Nollett K. M., Busso M., Wasserburg G. J., 2003, ApJ, 582, 1036

Parker R. J., Dale J. E., 2016, MNRAS, 456, 1066

Parker R. J., Goodwin S. P., 2007, MNRAS, 380, 1271

Parker R. J., Schoettler C., 2023, ApJ, 952, L16

Parker R. J., Nicholson R. B., Alcock H. L., 2021, MNRAS, 502, 2665

Parker R. J., Lichtenberg T., Patel M., Polius C. K. M., Ridsdill-Smith M., 2023, MNRAS, 521, 4838

Patel M., Polius C. K. M., Ridsdill-Smith M., Lichtenberg T., Parker R. J., 2023, MNRAS, 525, 2399

Pelupessy F. I., van Elteren A., de Vries N., McMillan S. L. W., Drost N., Portegies Zwart S. F., 2013, A&A, 557, A84

Portegies Zwart S. F., Verbunt F., 1996, A&A, 309, 179

Portegies Zwart S. F., McMillan S. L. W., van Elteren A., Pelupessy F. I., de Vries N., 2013, Comput. Phys. Commun., 184, 456

Qiao L., Coleman G. A. L., Haworth T. J., 2023, MNRAS, 522, 1939

Sánchez N., Alfaro E. J., 2009, ApJ, 696, 2086

Schmeja S., Klessen R. S., 2006, A&A, 449, 151

Schoettler C., Parker R. J., 2021, MNRAS, 501, L12

Schoettler C., de Bruijne J., Vaher E., Parker R. J., 2020, MNRAS, 495, 3104 Schoettler C., Parker R. J., de Bruijne J., 2022, MNRAS, 510, 3178 Tang H., Dauphas N., 2012, Earth Planet. Sci. Lett., 359, 248 Thrane K., Bizzarro M., Baker J. A., 2006, ApJ, 646, L159 Toonen S., Nelemans G., Portegies Zwart S., 2012, A&A, 546, id.A70 Trappitsch R., Ciesla F. J., 2015, ApJ, 805, 5 Trigo-Rodríguez J. M., García-Hernández D. A., Lugaro M., Karakas A. I., van Raai M., García Lario P., Manchado A., 2009, Meteorit. Planet. Sci., Trueman T. C. L., Côté B., Yagüe López A., den Hartogh J., Pignatari M., Soós B., Karakas A. I., Lugaro M., 2022, ApJ, 924, 10
Wasserburg G. J., Karakas A. I., Lugaro M., 2017, ApJ, 836, 126
Zwart S. P., McMillan S., 2018, Astrophysical Recipes: The Art of AMUSE. IOP Publishing, Bristol